PROCEEDINGS OF SPIE

SPIEDigitalLibrary.org/conference-proceedings-of-spie

Selective polarization generation in an amplifying photonic crystal with 2D array of metal nanoparticles

Sergey G. Moiseev, Yuliya S. Dadoenkova, Igor A. Glukhov, Tigran A. Vartanyan, Andrei A. Fotiadi, et al.

Sergey G. Moiseev, Yuliya S. Dadoenkova, Igor A. Glukhov, Tigran A. Vartanyan, Andrei A. Fotiadi, Florian F. L. Bentivegna, "Selective polarization generation in an amplifying photonic crystal with 2D array of metal nanoparticles ," Proc. SPIE 11031, Integrated Optics: Design, Devices, Systems, and Applications V, 1103114 (26 April 2019); doi: 10.1117/12.2520788

SPIE.

Event: SPIE Optics + Optoelectronics, 2019, Prague, Czech Republic

Selective polarization generation in an amplifying photonic crystal with a 2D array of metal nanoparticles

Sergey G. Moiseev,*[a,b] Yuliya S. Dadoenkova,[a] Igor A. Glukhov,[a,e] Tigran A. Vartanyan,[c]
Andrei A. Fotiadi,[a,d] Florian F. L. Bentivegna[e]

[a]Ulyanovsk State University, 42 Leo Tolstoy str., Ulyanovsk, Russia 432017
[b]Kotelnikov Institute of Radio Engineering and Electronics of the Russian Academy of Sciences, Ulyanovsk Branch, 48/2 Goncharov Str., Russia 432011
[c]ITMO University, 49 Kronverkskiy pr., St. Petersburg, Russia 197101
[d]Université de Mons, 20 Place du Parc, Mons, Belgium B-7000
[e]Lab-STICC (UMR 6285), CNRS, ENIB, CS 73862, Brest Cedex 3, France 29238

ABSTRACT

We show the possibility of polarization-selective amplification of a defect mode in an active photonic crystal through the excitation of surface plasmon resonance in a 2D periodic array of spheroidal metallic nanoparticles embedded in the structure. The array acts as a polarizer whose spectral characteristics depend on the shape of the nanoparticles and the periodicity of the array. The modal selectivity of the amplification is due to the strong dependence of the surface plasmon assisted light scattering by the nanoparticles on the relative orientations of their anisotropy axis and the polarization direction of the incoming light wave. We show that effective defect mode suppression, for a well-chosen polarization, can be achieved if the nanoparticles array is embedded in regions of high localization of the optical field.

Keywords: Nanoplasmonics; photonic crystal; defect mode; nanoparticles; field localization

1. INTRODUCTION

For many years photonic crystals (PC) have been the topic of intensive investigations. Owing to the periodic modulation of the refractive index in a PC, its transmission spectrum exhibits a photonic bandgap, i.e. a frequency interval for which electromagnetic waves cannot propagate through the structure. This property is of particular interest for practical uses since it allows the control of optical radiation, for instance in laser technology and data-transmission systems. By playing on the geometry, dimensions and constituents of PCs, it is possible to control their spectral characteristics [1] and to improve considerably their functionalities. For example, breaking the periodicity of the structure introduces one or several extremely thin transmission peaks in the photonic bandgap. Using materials whose optical response can be altered (*via* their non-linear, resonant, magneto-optical, etc., properties) allows further versatile control of the bandgap. Further interesting effects can be obtained by including metallic-dielectric nanocomposite media in a microcavity embedded in a PC. For instance, metallic nanoparticles (NPs) arranged in 2D or 3D arrays can efficiently modify the amplitude and the phase of an electromagnetic wave whose frequency is close to the plasmon resonance of the NPs [2-6]. The transmission spectra of such NP arrays depend on the nature of the metal, the size, shape and surface/volume ratio of the NPs, as well as the periodicity of the array. The use of composite media with non-spherical metallic NPs has been shown to allow a polarization-sensitive control of the resonance modes of PC-based structures [7, 8].

In this paper, we investigate theoretically the influence of a 2D array of metallic NPs placed in an amplifying defect layer in a 1D PC. We demonstrate that in order to obtain polarization-selective amplification of the defect mode, the 2D array should be placed in the regions of the maximal filed localization in the defect layer. We show that a maximal amplification or a nearly total suppression of the defect mode can be achieved, respectively for a polarization state of the incoming wave parallel or perpendicular to the long axis of the NPs.

*serg-moiseev@yandex.ru

Integrated Optics: Design, Devices, Systems, and Applications V, edited by Pavel Cheben, Jiří Čtyroký, Iñigo Molina-Fernández, Proc. of SPIE Vol. 11031, 1103114 · © 2019 SPIE · CCC code: 0277-786X/19/$18 · doi: 10.1117/12.2520788

2. DESCRIPTION OF THE SYSTEM AND GENERAL ANALYSIS

We consider a photonic structure composed of two distributed Bragg reflectors (DBRs) $(AB)^N$ and $(BA)^N$ separated by a composite microcavity (CDC) (Fig. 1), where A, B and C are layers of non-magnetic semiconductor materials, and D is an active (amplifying) region which ensures the amplification of electromagnetic waves propagating through the structure. The system is surrounded by vacuum, and we assume that an incident plane wave in the near-infrared regime impinges under normal incidence on the left-hand side of the structure, at $z = 0$ of a Cartesian coordinate system whose z-axis is perpendicular to the interfaces of the system. The time dependence of the electromagnetic fields is taken as $\exp(-i\omega t)$, where $\omega = 2\pi c/\lambda_0$ is the angular frequency of the incoming plane wave with wavelength in vacuum λ_0. The dimensions of the layers along the x- and y-axes are much larger than their thicknesses along the z-axis, so that the boundary effects along the x- and y- directions are neglected.

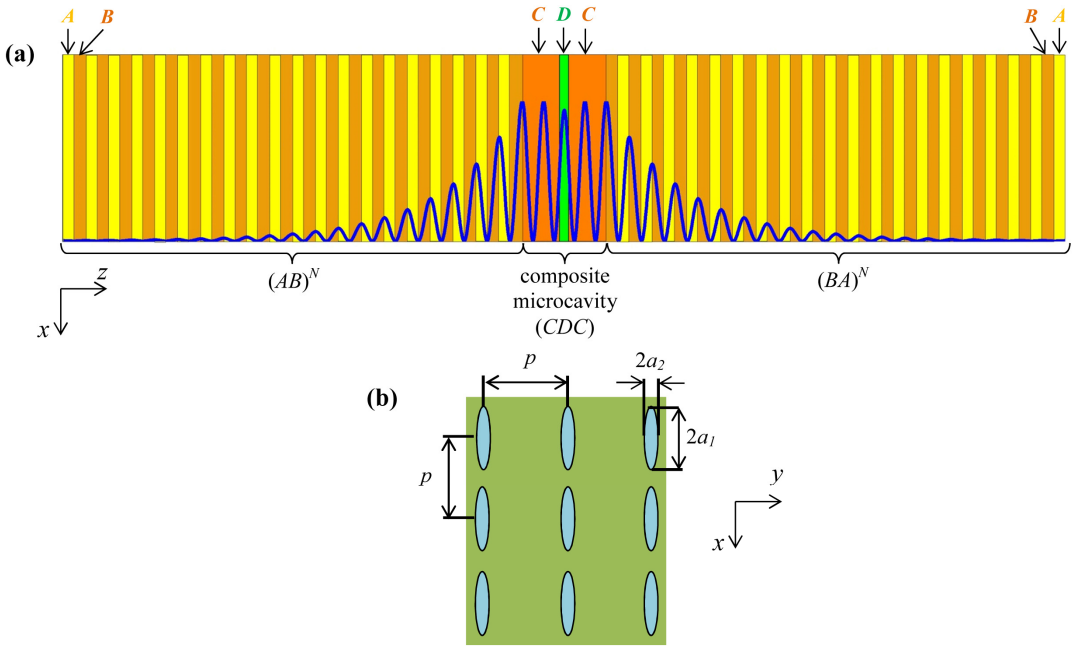

Figure 1. Schematic of the structure. (a) Two DBRs $(AB)^N$ and $(BA)^N$ are separated by a composite microcavity consisting of an amplifying layer D surrounded by two identical cladding layers C. The blue line shows the longitudinal distribution of the optical field intensity in the structure. (b) 2D array of metallic NPs. The distance between the centers of neighbouring NPs is p, and the lengths of the polar and equatorial axes of the NPs are $2a_1$ and $2a_2$, respectively.

Layers A and B are made of isotropic semiconductor materials GaAs and AlAs with dielectric permittivities ε_A and ε_B [9], respectively. Their thicknesses d_A = 115.5 nm and d_B = 134 nm satisfy the Bragg condition of resonant reflection $d_A\sqrt{\mathrm{Re}[\varepsilon_A]} = d_B\sqrt{\mathrm{Re}[\varepsilon_B]} = \lambda_0/4$ at $\lambda_0 = 1.55$ μm.

In the absence of microcavity, the transmission spectrum of the PC formed by the juxtaposition of those DBRs exhibits a photonic bandgap with a transmittivity peak, or defect mode centered on wavelength $\lambda_0 = 1.55$ μm because the central layer of a $(AB)^N(BA)^N$ PC (a so-called defect layer, with thickness $2d_B$), breaks the periodicity of the structure. Similarly, the presence of the (CDC) microcavity seen as a defect layer can introduce one or several defect modes inside the bandgap. Here, the cavity consists of two identical GaAs cladding layers (such that $\varepsilon_C = \varepsilon_A$ but with thickness $d_C = 404\,\mathrm{nm}$) surrounding an active region with an overall thickness $d_D = 104$ nm. This active region, similar to the structure described in Ref. [10], is a GaAs-based multiple quantum well VCSEL in which four $Ga_{0.591}In_{0.409}N_{0.028}As_{0.89}Sb_{0.08}$ quantum wells are separated by $GaN_{0.047}As$ barrier layers. The thicknesses of all those layers are chosen such that the microcavity introduces a single defect mode centered on wavelength $\lambda_0 = 1.55$ μm. If, as is the case here, the thicknesses of the layers composing the active region D are much smaller than λ_0, then it can be

described with good accuracy by an average dielectric permittivity $\varepsilon_D = \varepsilon_D' + i\varepsilon_D''$ obtained within the frame of an effective medium approximation [11]. Despite the optical absorption taking place in some of the layers of this VCSEL-based cavity, the active equivalent layer *D* provides an overall amplification of an electromagnetic wave around $\lambda_0 = 1.55$ μm, with $\varepsilon_D'' < 0$.

In the following, we assume that a single 2D array of spheroidal metallic NPs is placed inside the microcavity either in one of layers *C* or in layer *D*. All metallic NPs are identical and characterized by aspect ratio $\xi = a_1/a_2$ $(a_1 > a_2)$, where a_1 and a_2 are the half-lengths of their polar and equatorial axes, respectively. The NPs are ordered in a periodic 2D array with a square unit cell whose period *p* is the interparticle distance, such that the long axis of the NPs is parallel to the *x*-axis of the Cartesian coordinate system (see Fig. 1). Translational invariance is assumed along the *x* and *y* axes (see Fig. 1(b)). Note that $\{2a_1, 2a_2, p\} << \lambda_0 / \mathrm{Re}[\sqrt{\varepsilon_m}], m = \{C, D\}$. Such a structure exhibits pronounced anisotropic optical properties, and its reflection and transmission spectra depend significantly on the direction of polarization of the incident radiation [12, 13].

In order to calculate the spectral characteristics of the photonic structure with an embedded 2D array of NPs, we use the transfer matrix formalism. The transfer matrix of the whole structure is obtained through a sequential product of interface matrices (associated to either dielectric-dielectric interfaces or to the 2D array of NPs, i.e., $4N + 5$ interfaces in total) and propagation matrices (associated to the $4N + 4$ homogeneous layers sandwiched between consecutive interfaces). The transfer matrix for an internal interface separating two dielectric media with relative permittivities ε_{j-1} and ε_j, involves complex Fresnel reflection (r_j) and refraction (t_j) coefficients [14, 15]:

$$\hat{I}_j = \frac{1}{t_j}\begin{pmatrix} 1 & r_j \\ r_j & 1 \end{pmatrix},\ r_j = t_j - 1 = \frac{\sqrt{\varepsilon_{j-1}} - \sqrt{\varepsilon_j}}{\sqrt{\varepsilon_{j-1}} + \sqrt{\varepsilon_j}},\quad 2 \le j \le 4N+4. \tag{1}$$

The matrix associated to the first (respectively, last) interface of the system is similarly obtained with relative permittivities 1 and ε_A (respectively, ε_A and 1) on the left-hand (respectively, right-hand) side of the interface. The transfer matrix for an anisotropic 2D NP array, on the other hand, is expressed in terms of reflection coefficient $r_{x,y}^{\mathrm{NP}}$ that, even at normal indidence, depends on the polarization state of the incoming light wave. For the two orthogonal longitudinal (parallel to the *x*-axis) and transverse (parallel to the *y*-axis) polarization states, these coefficients and the corresponding interface matrix for the NP array are [16]:

$$\hat{I}_{x,y}^{NP} = \frac{1}{1 + r_{x,y}^{NP}}\begin{pmatrix} 1 & -r_{x,y}^{NP} \\ r_{x,y}^{NP} & 1 + 2r_{x,y}^{NP} \end{pmatrix},\qquad r_{x,y}^{\mathrm{NP}} \approx i\frac{k_0\sqrt{\varepsilon_m}}{2p^2}\alpha_{x,y} \tag{2}$$

where $\alpha_{x,y} = V(\varepsilon_p - \varepsilon_m)/\left(g_{x,y}(\varepsilon_p - \varepsilon_m) + \varepsilon_m\right)$ is the complex polarizability of an individual spheroidal NP in an external optical field applied along the *x*- or *y*-axis, $k_0 = 2\pi/\lambda_0$ is the wavevector in vacuum, ε_p and ε_m are relative permittivities of the NP and surrounding medium, respectively, $V = 4\pi a_1 a_2^2/3$ is the volume of the NP, and $g_{x,y}$ is a geometric factor accounting for the influence of the shape of the NP on its induced dipolar moment, with $g_x = \left(1-\xi^2\right)^{-1}\left(1 - \xi\left(1-\xi^2\right)^{-1/2}\arcsin\left(1-\xi^2\right)^{1/2}\right)$ and $g_y = (1 - g_x)/2$ [17].

The optical fields at two adjacent interfaces j^{th} and $(j+1)^{\mathrm{th}}$ surrounding the j^{th} homogeneous layer *j* are related via the propagation matrix $\hat{F}_j$ defined as [14]:

$$\hat{F}_j = \begin{pmatrix} \exp(-ik_0\sqrt{\varepsilon_j}d_j) & 0 \\ 0 & \exp(ik_0\sqrt{\varepsilon_j}d_j) \end{pmatrix}. \tag{3}$$

Overall, the complex amplitudes of the incident E_i, reflected E_r, and transmitted E_t optical fields are related through the transfer matrix $\hat{G}_{x,y} = \hat{I}_1\hat{F}_1\hat{I}_2\hat{F}_2\cdots\hat{I}_{x,y}\cdots\hat{F}_{4N+4}\hat{I}_{4N+5}$ of the entire structure, with

$$\begin{pmatrix} E_i \\ E_r \end{pmatrix} = \hat{G}_{x,y} \begin{pmatrix} E_t \\ 0 \end{pmatrix}, \tag{4}$$

and the reflectivity and transmittivity of the system are obtained as

$$T = |E_t / E_i|^2 = \left|\hat{G}_{11}\right|^{-2}, \qquad R = |E_r / E_i|^2 = T\left|\hat{G}_{21}\right|^2. \tag{5}$$

3. NUMERICAL RESULTS AND DISCUSSION

For the numerical calculations discussed in this Section, we take the following values for the dielectric permittivities of the PC layers at $\lambda_0 = 1.55$ μm: $\varepsilon_A \approx 11.255 + i0.027$, $\varepsilon_B \approx 8.36$ [9], $\varepsilon_D \approx 12.869 - i0.214$ [10]. The NPs are made of silver (Ag) and their relative permittivity is taken to follow the Drude model, with $\varepsilon_p(\omega) = \varepsilon_\infty - \omega_p^2 / \left(\omega^2 + i\omega\gamma\right)$, where $\omega_p = 1.35\times10^{16}$ rad·s^{-1} is the plasma frequency in silver, $\varepsilon_\infty = 5$ is the contribution of its crystal lattice, and $\gamma = 5.5\times10^{13}$ s^{-1} is the relaxation rate describing the effective electron scattering rate in that crystal [18]. The length of the polar axis of NPs is $2a_1 = 20$ nm, the aspect ratio of the NPs is $\xi = 3.6$, and the period of the NP array is $p = 90$ nm.

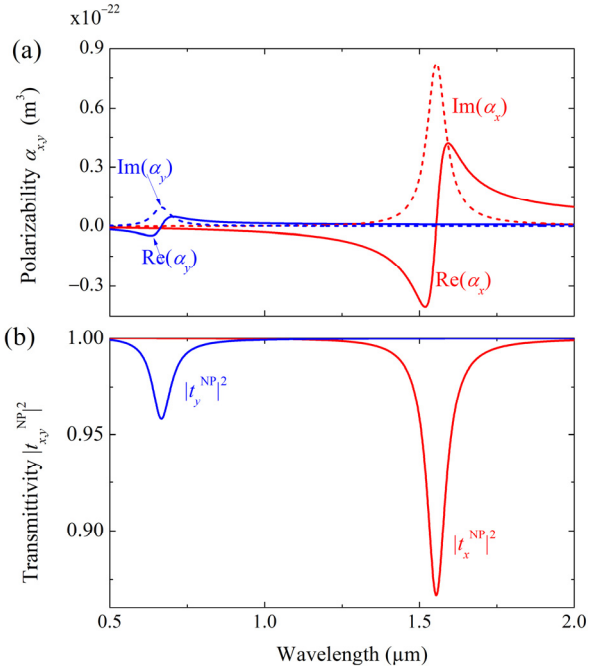

Figure 2. Spectra of (a) polarizability of a single NP and (b) transmittivity of a 2D array of NPs embedded in a GaAs matrix for the longitudinal (x-) and transverse (y-) polarization states of the incoming light wave.

First we illustrate the spectral properties of the NP array. Figures 2(a) and 2(b) show the polarizability $\alpha_{x,y}$ and transmittivity $|t_{x,y}^{\mathrm{NP}}|^2 = |1 + r_{x,y}^{\mathrm{NP}}|^2$ spectra of the 2D NP array for the longitudinal and transverse components of the incoming light field. Dips in the transmittivity spectra correspond to wavelengths coinciding with the resonant excitation of surface plasmons in the spheroidal silver particles. Due to the anisotropy of the particles, these resonances do not occur at the same wavelength for longitudinal and transverse polarization states ($\lambda_0 = 1.55$ μm and $\lambda_0 = 0.67$ μm, respectively). The amplitude of the plasmon resonance is also approximately twice larger for longitudinally polarized light, for which the dipolar moment induced in each NP is larger than for transversally polarized light. This can be associated with the respective values of polarizabilities $|\alpha_x| > |\alpha_y|$ (see Fig. 2(a)) for prolate spheroids ($\xi > 1$) aligned as in Fig. 1, hence a better efficiency of the coupling of the optical electric field with surface plasmons for the longitudinal polarization.

Let us now consider the active structure without embedded 2D NP array (Fig. 1(a)). As expected, its transmittivity spectrum (Fig. 3) exhibits a photonic bandgap and a defect mode centered on $\lambda_0 = 1.55$ µm. Due to the presence of the active composite microcavity, the transmittivity associated with that defect mode greatly exceeds 1 (see inset in Fig. 3). This structure does not contain any anisotropic element, so that the defect mode amplification does not depend on the polarization state of the incoming light. The spatial distribution of the optical intensity along the *z*-axis, obtained with transfer matrix calculations (solid blue line in in Fig. 1(a)) shows five maxima within the (*CDC*) microcavity: one local maximum at the center of the active layer *D* and two larger maxima symmetrically located on each side of that center.

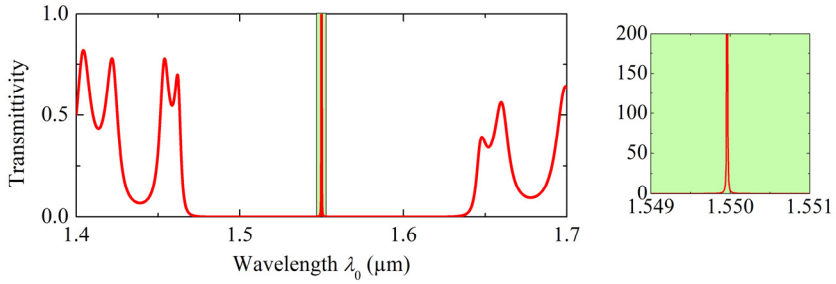

Figure 3. Transmittivity spectrum of the photonic structure without NP array. The spectrum is identical for any direction of the plane of polarization of the incident light wave. The inset zooms in on the spectrum around the defect mode (note the different vertical scales in the inset and in the main figure).

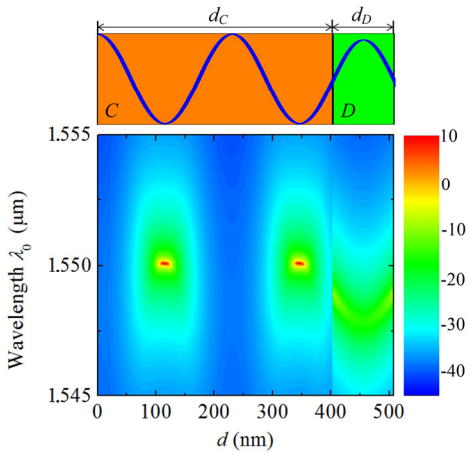

Figure 4. Evolution of the transmittivity spectrum T_x (in dB) of the photonic structure, in the vicinity of the defect mode, with the position of the 2D array of NPs across layers *C* and *D* of the composite microcavity. The top inset shows the field intensity distribution in layers *C* and *D*.

When the NP array is embedded at any location within the (*CDC*) microcavity, the transmittivity spectrum T_y of the transverse polarization remains virtually identical to that shown in Fig. 3. This is evidently due to the fact that in this case, the wavelength of the incoming light is too far from the wavelengths of the plasmon resonances (blue lines in Fig. 2) to be able to excite them, so that the presence of the NP array does not significantly affect the amplification of the defect mode for a *y*-polarized light.

On the contrary, for the *x*-polarized light the position of the defect mode coincides with the surface plasmon resonance (see Figs. 2 and 3). In this case the transmittivity spectrum T_x is very sensitive to the position of the NP array, and the defect mode can be suppressed. Figure 4 shows the evolution of the transmittivity spectrum of the *x*-polarized light, in the vicinity of the defect mode, with the position of the NP array in the layers *C* and *D* of the microcavity. When the NP array is embedded at locations of maximal field localization, the defect mode vanishes (NP array located at one of the intensity maxima in the layer *C*) or at least significantly reduced (NP array located at the center of the layer *D*). In the latter case, the defect mode also exhibits a blue shift. On the contrary, when the NP array is placed in the region of minimal field localization, the plasmon resonance is not excited and the defect mode is amplified, like for the *y*-polarization of light.

4. CONCLUSIONS

We have demonstrated that polarization-controlled amplification of a defect mode can be achieved in an amplifying photonic crystal in which a 2D array of silver nanoparticles is embedded. The nonspherical shape of the nanoparticles ensures the suppression of the defect mode for incoming light polarized such that it can excite their plasmon polariton resonance. The suppression of the defect mode is most efficient when the nanoparticle array is embedded at locations of maximal optical field localization in the amplifying region of the structure.

ACKNOWLEDGEMENTS

The authors thank the Ministry of Science and Higher Education of the Russian Federation (3.5698.2017/9.10, 3.7614.2017/9.10), the Russian Foundation for Basic Research and the government of Ulyanovsk region (18-42-730007, 18-29-19101), the Russian Science Foundation (grant №18-12-00457), the École Nationale d'Ingénieurs de Brest, France (HF-CCCP), and the Regional Council of Brittany, France (PhotoMag) for their support. A.F. acknowledges a support from the Leverhulme Trust (Visiting Professor, Grant ref: VP2-2016-042).

REFERENCES

[1] Gong, Q. and Hu, X., [Photonic Crystals: Principles and Applications], Pan Stanford, Boca Raton (2014).
[2] Ding, F., Pors, A. and Bozhevolnyi, S. I., "Gradient metasurfaces: a review of fundamentals and applications," Rep. Prog. Phys. 81, 026401 (2018).
[3] Kullock, R., Grafström, S., Evans, P. R., Pollard, R. J. and Eng, L. M., "Metallic nanorod arrays: negative refraction and optical properties explained by retarded dipolar interactions," J. Opt. Soc. Am. B 27, 1819-1827 (2010).
[4] Moiseev, S. G., "Active Maxwell–Garnett composite with the unit refractive index," Physica B 405, 3042-3045 (2010).
[5] Dadoenkova, Y., Glukhov, I., Moiseev, S., Svetukhin, V., Zhukov, A. and Zolotovskii, I., "Optical generation in an amplifying photonic crystal with an embedded nanocomposite polarizer," Opt. Commun. 389, 1-4 (2017).
[6] Rahachou, A. I. and Zozoulenko, I. V., "Light propagation in nanorod arrays," J. Opt. A: Pure Appl. Opt. 9, 265–270 (2007).
[7] Moiseev, S. G., Ostatochnikov, V. A. and Sementsov, D. I., "Defect mode suppression in a photonic crystal structure with a resonance nanocomposite layer," Quantum Electron. 42, 557-560 (2012).
[8] Vetrov, S. Ya., Bikbaev, R. G. and Timofeev, I. V., "The optical Tamm states at the edges of a photonic crystal bounded by one or two layers of a strongly anisotropic nanocomposite," Opt. Commun. 395, 275-281 (2016).
[9] Rakić, A. D., Majewski, M. L., "Modeling the optical dielectric function of GaAs and AlAs: Extension of Adachi's model," J. Appl. Phys. 80, 5909-5914 (1996).
[10] Rahman, M. A., Karim, M. R., Akhtar, J. and Reja, M. I., "Performance characterization of a GaAs based 1550 nm Ga0.591In0.409N0.028As0.89Sb0.08 MQW VCSEL," Int. J. of Photonics and Opt. Techn. 4, 14-18 (2018).
[11] Sihvola, A., [Electromagnetic Mixing Formulas and Applications], The Institution of Electrical Engineers, London (1999).
[12] Moiseev, S. G., "Nanocomposite-based ultrathin polarization beamsplitter," Opt. Spectrosc. 111, 233-240 (2011).
[13] Lozovski, V. and Razumova, M., "Influence of inclusion shape on light absorption in thin Au/Teflon nanocomposite films," J. Opt. Soc. Am. B 33, 8-16 (2016).
[14] Katsidis, C. C. and Siapkas, D. I., "General transfer-matrix method for optical multilayer systems with coherent, partially coherent, and incoherent interference," Appl. Opt. 41(19), 3978-3987 (2002).
[15] Born, M. and Wolf, E., [Principles of Optics], Cambridge University Press, Cambridge (1999).
[16] Holloway, C. L., Mohamed, M. A., Kuester, E. F. and Dienstfrey A., "Reflection and transmission properties of a metafilm: With an application to a controllable surface composed of resonant particles," IEEE Trans. Electromagn. Compat. 47(4), 853–865 (2005).
[17] Bohren, C. F. and Huffman, D. R., [Absorption and Scattering of Light by Small Particles], Wiley, New York (1983).
[18] Yang, H. U., D'Archangel, J., Sundheimer, M. L., Tucker, E., Boreman, G. D. and Raschke, M. B., "Optical dielectric function of silver," Phys. Rev. B 91, 235137 (2015).